Effect of Superheat on the Solidification Structures of AISI 310S Austenitic Stainless Steel

S. OZBAYRAKTAR and A. KOURSARIS

An experimental study was carried out to investigate the evolution of macrostructure and microstructure in AISI 310S stainless steel during solidification. Experimental findings suggested that the macrostructure and the microstructure of the cast material responded differently to variations in casting temperature. As the casting temperature decreased, the macrostructure was refined, as expected, but the microstructure coarsened. A relationship was established between the proportion of equiaxed zone and superheat as follows:

$$\text{pct equiaxed zone} = a + b \ln (1/\Delta T)$$

where a and b are constants. The relationship between grain width and superheat could be expressed by the equation

$$gw = e^{(c+d/\Delta T)}$$

where c and d are constants determined by the distance from the edge of the ingot. The relationship between primary arm spacing and superheat could be expressed by the equation

$$\lambda_1 = p + q \ln (1/\Delta T)$$

where p and q are constants determined by the distance from the edge of the ingot. The parameter "grain width ratio" has been introduced to describe the relationship between the shape and the nucleation and growth kinetics of the columnar grains.

I. INTRODUCTION

THE solidification parameters that determine the nature of the cast structure are the thermal gradient, growth rate, and alloy variables such as the slope of the liquidus, solute distribution coefficient, and initial solute concentration.

The ratio of thermal gradient (G) to growth rate (R) has been shown to be a significant parameter with respect both to the mode of growth and the final grain structure produced in solid solution alloys.[1-5]

In his extensive work on AISI 310S stainless steel, Fiegenschuh[6] studied the effects of casting temperature and cooling rate on the cast structure of this material. He observed an exponential relationship between casting temperature and average grain size at constant cooling rate (40 $Kmin^{-1}$). He derived the following relation between the cooling rate and the average grain size:

$$d_m = 13.66v^{-0.16} \quad [1]$$

where d_m is the average grain size and v the cooling rate in Kh^{-1}. This equation was based on an earlier model[6] which is of the form

$$d_m^{1/2} = k' v_L^n \quad [2]$$

where k' and n are constants and v_L is the linear cooling rate at the liquidus point of the alloy.

The cooling rates employed by Fiegenschuh[6] in his casting experiments were relatively slow compared to cooling rates prevailing during continuous casting. The cooling rate could be as high as 1440 Ks^{-1} at 0.5 mm from the surface of continuous cast slabs. It drops sharply to about 360 Ks^{-1} at 1 mm and to about 75 Ks^{-1} at 3 mm from the surface.[7] At high cooling rates, AISI 310S was found[8] to solidify through a peritectic reaction rather than directly to austenite.

Although the effect of casting temperature on the evolution of macrostructure is well documented, its effect on the microstructure of cast steels has not been explored in detail. It was expected that as the macrostructure was refined, the microstructure should change likewise.[9] However, in his work on the effects of nucleation and constitutional supercooling on the properties of cast steel, Church[10] showed that higher casting temperatures resulted in smaller primary and secondary arm spacings. He found that cooling rates for the castings poured from higher temperatures were greater, resulting in a shorter mushy zone due to steeper thermal gradients in the liquid-solid region.

In this work, the effect of superheat on the as-cast macro- and microstructure at high cooling rates was investigated to gain a fuller understanding of the processes involved in the solidification of austenitic stainless steels. This understanding, in turn, will form the basis of a solidification model for AISI 310S.

II. EXPERIMENTAL PROCEDURE

The principal experimental procedure aimed to study the solidification process of AISI 310S stainless steel by investigating the macro- and microstructural changes that

S. OZBAYRAKTAR, Senior Research Scientist, is with De Beers Diamond Research Laboratories, Johannesburg, 2000 South Africa. A. KOURSARIS, Associate Professor, is with the School of Process and Materials Engineering, University of the Witwatersrand, Johannesburg, 2050 South Africa.

Manuscript submitted October 8, 1994.

Table I. Chemical Composition of the AISI 310S Stainless Steel

Pct C	Pct S	Pct P	Pct Mn	Pct Si	Pct Cu	Pct Co	Pct Ti	Pct Mo
0.047	0.005	0.026	1.67	0.46	0.070	0.040	0.008	0.010
	Pct V	Pct Nb	Pct Al	Pct B	Pct Cr	Pct Ni	N_2 ppm	O_2 ppm
	0.12	0.001	0.013	0.002	24.48	19.24	177	64

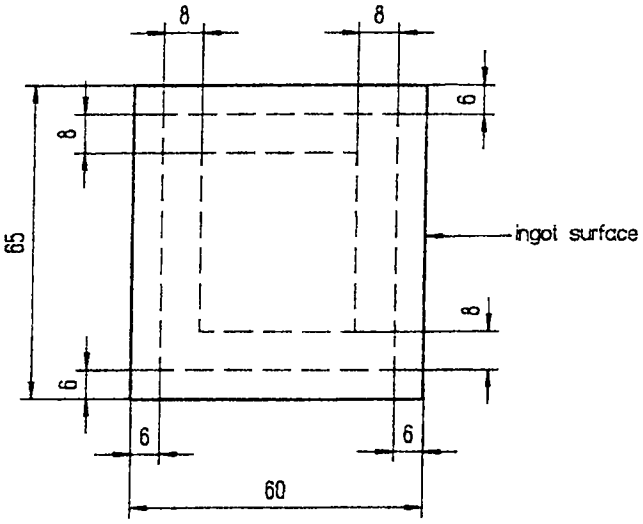

Fig. 1—Concentric squares used to measure the grain widths. Dimensions in millimeters.

take place when the alloy is cast with different amounts of superheat is discussed in the remainder of this section.

A. *Materials and Melting Practice*

Strips of stainless steel AISI 310S, whose chemical composition is given in Table I, were cut into sizes to fit in the melting crucible and cleaned by sand blasting to remove the oxide layer, dirt, and other contaminants from the surface.

A vacuum induction melting furnace capable of delivering 100 kW at 3000 Hz and a built-in sintered magnesia crucible were used to melt the material. The molten metal was poured into flake graphite cast iron molds of 6 kg capacity placed on a water-cooled mold table. The melting and casting were done under an argon atmosphere which was held at 500 mbars for all castings.

The temperature of the molten metal was measured with a Pt-6 pct rhodium/Pt-30 pct rhodium thermocouple which was inserted into the furnace through a built-in air-tight inlet.

Once the metal had melted, the thermocouple was dipped into the melt to record the temperature. Heating was continued to a predetermined degree of superheat when the power was switched off and the melt allowed to cool down to the casting temperature for that specific ingot. The alloy was then poured into ingots of 65 × 65 × 250 mm size and allowed to cool in the furnace.

Sixteen ingots were cast to determine the influence of casting temperature on macro- and microstructure and on the solidification mode of AISI 310S.

B. *Cooling Rates during Solidification*

Suzuki and Nakaoka[11] derived the following empirical relationship for secondary arm spacing for AISI 310S steel:

$$\lambda_2 = 44R^{-0.38} \quad [3]$$

where λ_2 is the secondary dendrite arm spacing in micrometers and R is the cooling rate in Ks^{-1}. This relationship was used to calculate the cooling rates of the ingots cast for the present work. The results showed that the cooling rates at 2 mm from the edge varied from 23 Ks^{-1} (1380 $Kmin^{-1}$) for ingots cast from 1610 °C to 5 Ks^{-1} (300 $Kmin^{-1}$) for ingots cast from 1493 °C.

C. *Macrostructural Examination of the As-Cast Structures*

Three transverse slices were cut from each ingot and used for chemical analyses and micro- and macrostructural examinations. Hot mixed acid solution (38 pct HCl, 12 pct H_2SO_4, and 50 pct H_2O) was used to reveal the macrostructure. After etching, the surfaces were examined visually to determine the effect of superheat on the macrostructure. The width of the columnar grains was determined by the linear intercept method in which the number of grains intersected by the perimeters of "concentric" squares was determined (Figure 1). The dimensions of the outer square were chosen such that the chill zone was excluded from measurements. The grain width measurements were taken at 6 and 14 mm from the edges of the transverse slices.

The grains were counted at least five times for each ingot, and a statistical analysis was performed to ensure that at the 95 pct confidence limit, the variance of the counts did not exceed 10 pct.

D. *Microstructural Examination of the As-Cast Structures*

One slice from each ingot was ground on successively finer grades of carbide paper up to 1200 grit. Final polishing was done by use of 3- and 1-μm diamond lapping compounds. An electrolytic etch in oxalic acid was used to reveal the microstructure which was examined with the optical microscope.

Primary dendrite arm spacings were measured at intervals of 2 mm from two opposite edges of the slice. A statistical analysis was performed to calculate the error and the reliability of the measurements. For the primary arm spacings, the 95 pct confidence limits were within ± 15 pct of the average values. The confidence limits for primary arm spacings increased with increasing distance from the edge, indicating a greater degree of scatter in the measurements. This was due to the fact that dendritic growth is competitive and the dendrites coarsened with increasing

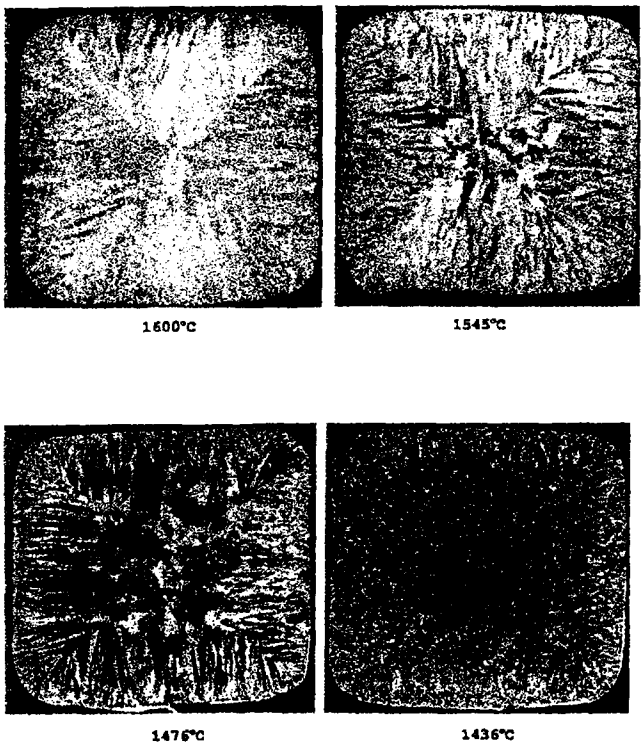

Fig. 2—Macrostructures of ingots cast from different temperatures.

distance from the edge. Thus, measurements were taken from fewer dendrites. Control measurements were made on the same samples about 3 months later to examine whether the new mean values obtained would fall within the confidence limits. This was found to be the case, indicating that the original measurements were reliable.

The measurements of primary arm spacings determined at intervals of 2 mm as described previously were used to work out the primary arm spacings at 10 and 15 mm from the edge.

III. EXPERIMENTAL RESULTS

A. *Ingot Macrostructure*

The transverse sections of selected ingots cast from temperatures between 1436 °C and 1610 °C are shown in Figure 2. The results of the measurements on ingot macrostructures are given in Table II.

The relationship between the columnar grain widths and the degree of superheat was analyzed and could be expressed by the equations:

$$\ln(\text{grain width at 6 mm}) = 5.66 + 6.36*10^{-3}\Delta T \quad [4]$$

$$\ln(\text{grain width at 14 mm}) = 6.05 + 5.25*10^{-3}\Delta T \quad [5]$$

Grain width is in micrometers, and ΔT is superheat in degree Celsius.

The change in grain width at 6 and 14 mm with changing degree of superheat and the regression curves are shown in Figure 3. This figure demonstrates that the slope of the plot of grain width against superheat is a function of the distance from the edge of the ingot. As can be seen, the two lines converge with increasing superheat.

It was evident that as the casting temperature decreased, the grain size of the columnar zone decreased and the volume of the equiaxed zone increased. At casting temperatures below about 1450 °C, corresponding to a superheat of about 50 °C, the equiaxed zone started to dominate the macrostructure, as can be seen from Figure 2.

The development of the equiaxed zone with changing superheat is shown in Figure 4. It can be seen that the proportion of equiaxed zone decreased rapidly as the degree of superheat increased from 36 °C to about 100 °C. A small equiaxed zone, however, persisted with further increase in superheat. The proportion of the equiaxed zone was about 5 pct for superheat values of about 160 °C to 170 °C.

When the proportion of equiaxed zone was plotted against the inverse of superheat on a semilog scale, as shown in Figure 5, a strong correlation was found between the two (correlation coefficient = 0.95) in the temperature range 1436 °C to 1564 °C. This could be expressed by the equation

$$\text{pct equiaxed zone} = 244.5 + 49.4 \ln(1/\Delta T) \quad [6]$$

where ΔT = superheat in degrees Celsius.

The grain width measured at a distance of 14 mm from the edge was divided by the grain width measured at 6 mm from the edge of the ingots to determine the grain width ratio for each ingot (Table II). The grain width ratios were plotted against casting temperature (Figure 6) and showed that as the pouring temperature increased, the grain width ratio decreased. This means that in ingots cast with low superheat, the width of columnar grains increased as they grew toward the center of the ingot. The width of grains in ingots cast with high superheat did not change significantly as these grew toward the center of the ingot. Expressed simply, these observations show that the nucleation and growth behavior of columnar grains depend on the degree of superheat. The significance of this is discussed in Section IV.A.

When the grain width ratio was plotted against the grain width measured at 14 mm (Figure 7), it could be seen that as the grain width decreased, the grain width ratio increased.

B. *Results of the Microstructural Evaluation of the As-Cast Ingots*

The measurements of dendrite arm spacing indicated that there is a strong relationship between casting temperature and primary arm spacing (Figure 8), whereas it seemed that the secondary arm spacing at distances of 10 and 15 mm from the edge of the ingots was insensitive to casting temperature variations (Figure 9).

When the data for primary arm spacings were analyzed statistically, the following equations were derived for spacings at 6 and 14 mm from the edge of ingots:

$$\lambda_1\ (6\text{ mm}) = 0.04733 + 0.007354 \ln \frac{1}{\Delta T} \quad [7]$$

$$\lambda_1\ (14\text{ mm}) = 0.09485 + 0.01480 \ln \frac{1}{\Delta T} \quad [8]$$

where λ_1 is the primary dendrite arm spacing in centimeters and ΔT is the superheat.

Table II. Change in Macrostructure with Casting Temperature

Ingot Number	Casting Temperature (°C)	Columnar Grain Width (mm) with 95 Pct Confidence Limits Measured at 6 and 14 mm from the Edge		Grain Width Ratio (gw at 14 mm/ gw at 6 mm)	Equiaxed Zone (Pct)
		6 mm	14 mm		
B1	1610	1.140 ± 0.119	1.330 ± 0.050	1.17	0
B2	1600	1.055 ± 0.145	1.134 ± 0.178	1.07	3
B3	1585	1.047 ± 0.092	1.204 ± 0.069	1.22	0
B4	1564	0.844 ± 0.062	1.030 ± 0.080	1.15	4
B5	1545	0.666 ± 0.082	0.920 ± 0.080	1.38	3
B6	1537	0.711 ± 0.107	0.975 ± 0.129	1.37	4
B7	1526	0.551 ± 0.059	0.704 ± 0.054	1.28	7
B8	1520	0.517 ± 0.082	0.710 ± 0.098	1.37	10
B9	1510	0.498 ± 0.059	0.672 ± 0.072	1.35	13
B10	1502	0.456 ± 0.046	0.647 ± 0.013	1.42	8
B11	1496	0.511 ± 0.049	0.669 ± 0.093	1.31	7
B12	1493	0.749 ± 0.091	0.920 ± 0.012	1.23	13
B13	1476	0.434 ± 0.042	0.666 ± 0.066	1.53	23
B14	1455	0.482 ± 0.049	—	—	50
B15	1436	0.365 ± 0.051	—	—	77

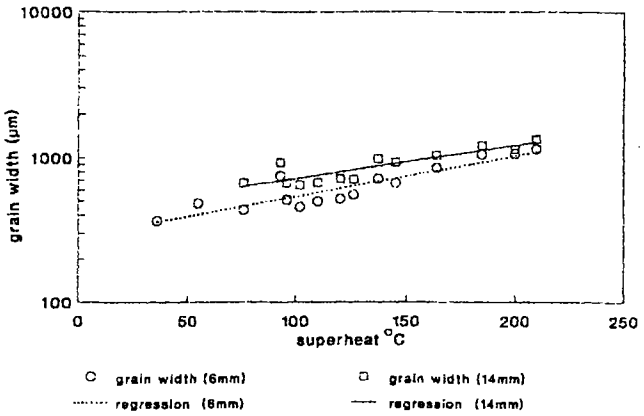

Fig. 3—Plots of grain width at 6 and 14 mm from the edge of ingots against superheat.

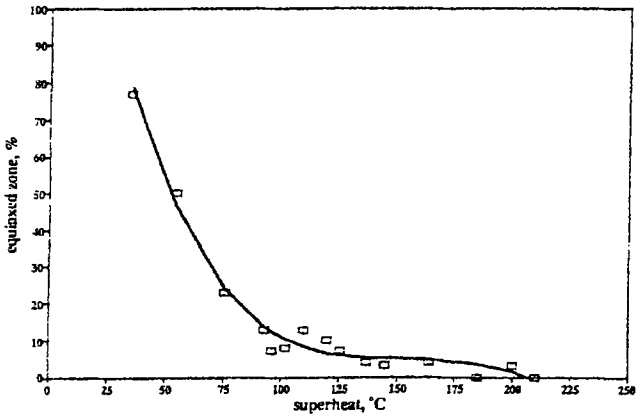

Fig. 4—Influence of superheat on the proportion of equiaxed zone.

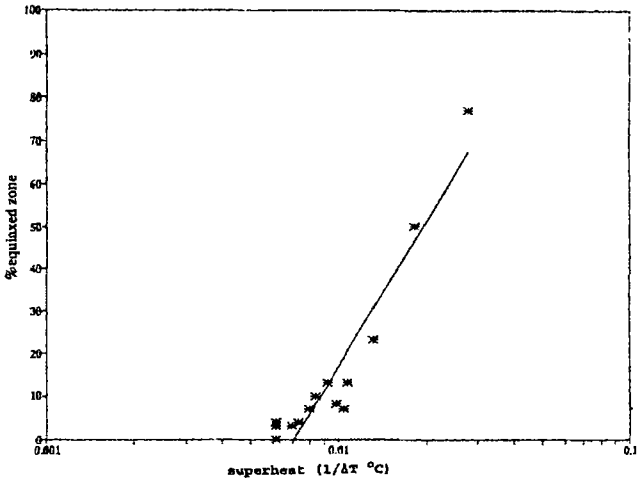

Fig. 5—Change in the proportion of the equiaxed zone with superheat.

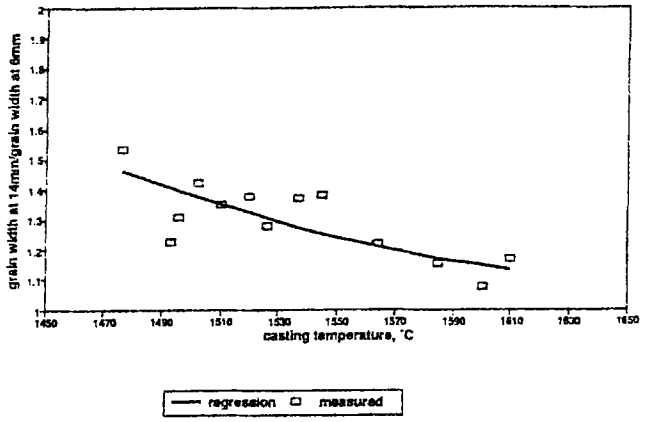

Fig. 6—Change in grain width ratio (gw_{14}/gw_6) with casting temperature.

Figure 8 shows that as the casting temperature was increased, the primary dendrite arm spacing decreased. In other words, the microstructure was refined by pouring from higher temperatures. This is also evidenced by the micrographs taken at various distances from the edges of these ingots (Figures 10 and 11). As can be seen from these micrographs, the number of primary arms comprising one macrograin, in castings poured from high temperatures, was a few times larger than that of castings poured from lower temperatures.

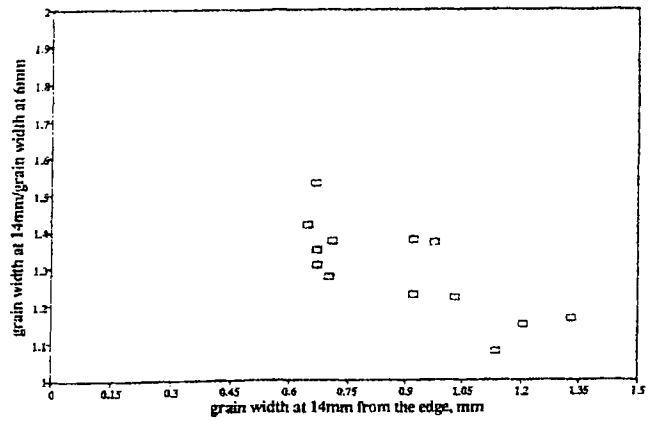

Fig. 7—Change in grain width ratio with grain width at 14 mm.

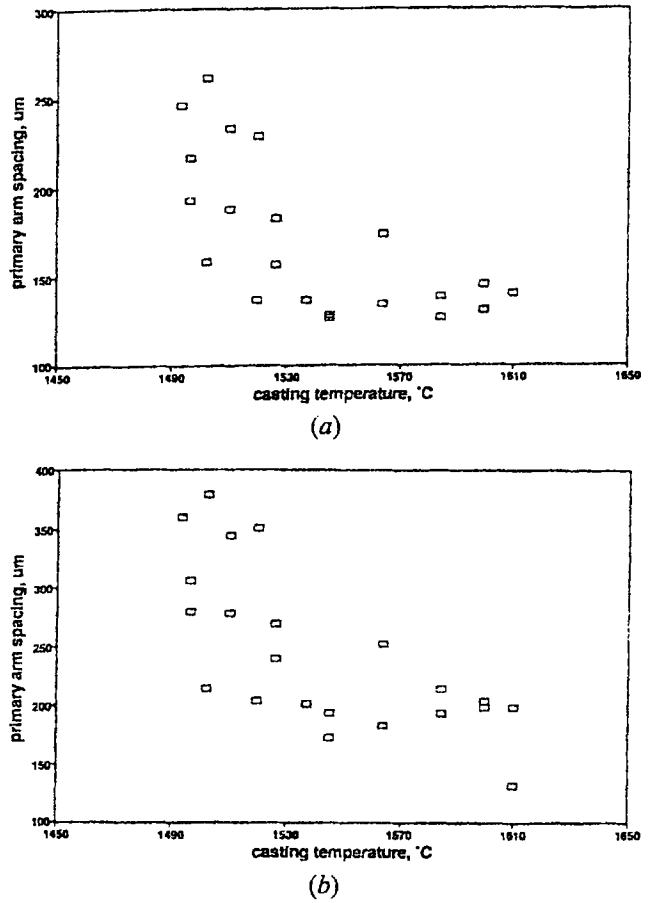

Fig. 8—Variation in primary dendrite arm spacing with casting temperature measured at (*a*) 10 mm and (*b*) 15 mm from the chill zone.

Comparison between the microstructures of ingot B2 cast from 1600 °C and ingot B11 cast from 1496 °C will demonstrate the point. The primary dendrite arm spacings were 140 and 210 μm, respectively, at 10 mm from the chill zone. However, columnar grain width measurements for the same ingots gave 1.055 and 0.511 mm, respectively, at 6 mm from the chill zone (Table II). In castings poured from low temperatures, the number of columnar grains was higher but the number of primary dendrite arms in these grains was lower. The result was a coarser primary arm spacing in ingots cast from lower temperatures.

These opposing trends of primary arm spacings and columnar grain widths with casting temperature became obvious when they were plotted against each other (Figure 12).

It can be seen that the primary arm spacing decreased with increasing columnar grain width. A rapid rate of change was noted for columnar grain widths of 0.4 to 0.8 mm. Above 0.8 mm, the dendrite arm spacing appeared to remain constant at about 190 to 200 μm. These trends corresponded to casting temperature ranges of 1470 °C to 1545 °C and 1545 °C to 1610 °C, respectively.

The changes in secondary arm spacing with changes in primary arm spacing were initially analyzed separately for castings in which a temperature effect on this relationship suggested itself. In order to simplify matters, the data were grouped into two temperature ranges in which the cutoff temperature between the two was decided after a careful analysis of the slopes obtained by regression analyses of each ingot sample. These two power curves were plotted together with curves for other alloys found in the literature (Figure 13). As can be seen, the higher the casting temperature, the larger the secondary dendrite arm spacing per unit primary arm spacing. This confirms the results discussed previously, which showed refinement in the primary arm spacing as the casting temperature was increased. It can also be said that the secondary arm spacing was not very sensitive to thermal gradient effects during solidification.

IV. DISCUSSION

A. *Effect of Superheat on the As-Cast Macrostructure of AISI 310S Stainless Steel*

The results of this study showed that the width of the columnar grains and the proportion of the columnar zone decreased with decreasing superheat, while the proportion of the equiaxed zone increased.

The relationship between grain width and superheat was modeled by use of logarithmic expressions despite the fact that second and fourth degree polynomials were found to give slightly higher correlation coefficients. The choice of logarithmic expressions was based on the fact that they fitted the data well and facilitated the modeling process. The interesting phenomenon observed here was that the grain widths measured at 6 and 14 mm from the edge changed at different rates as the degree of superheat was varied. This observation suggested the introduction of the parameter grain width ratio, which is defined as the ratio of grain width at 14 mm to grain width at 6 mm from the edge of the ingot. This ratio proved to be quite useful in describing the nucleation and growth characteristics of columnar structures.

As can be seen from Figure 6, the grain width ratio increased as the casting temperature was decreased. This phenomenon can best be explained by considering the changes that take place in the nucleation and growth rates of γ grains in this temperature range, as illustrated in Figure 14.

Ingots cast in the high-temperature casting range (1565 °C to 1610 °C) showed coarse columnar grains. In this range, the superheat was so high that the crystals that nucleated initially were remelted by the heat in the liquid after the initial chilling at the mold walls.

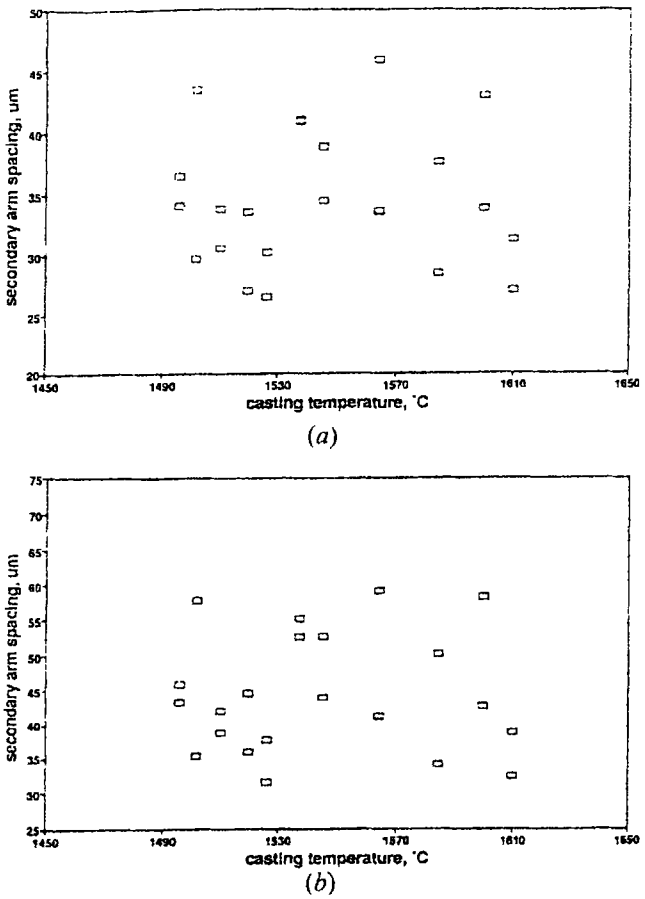

Fig. 9—Variation in secondary dendrite arm spacings with casting temperature measured at (*a*) 10 mm and (*b*) 15 mm from the chill zone.

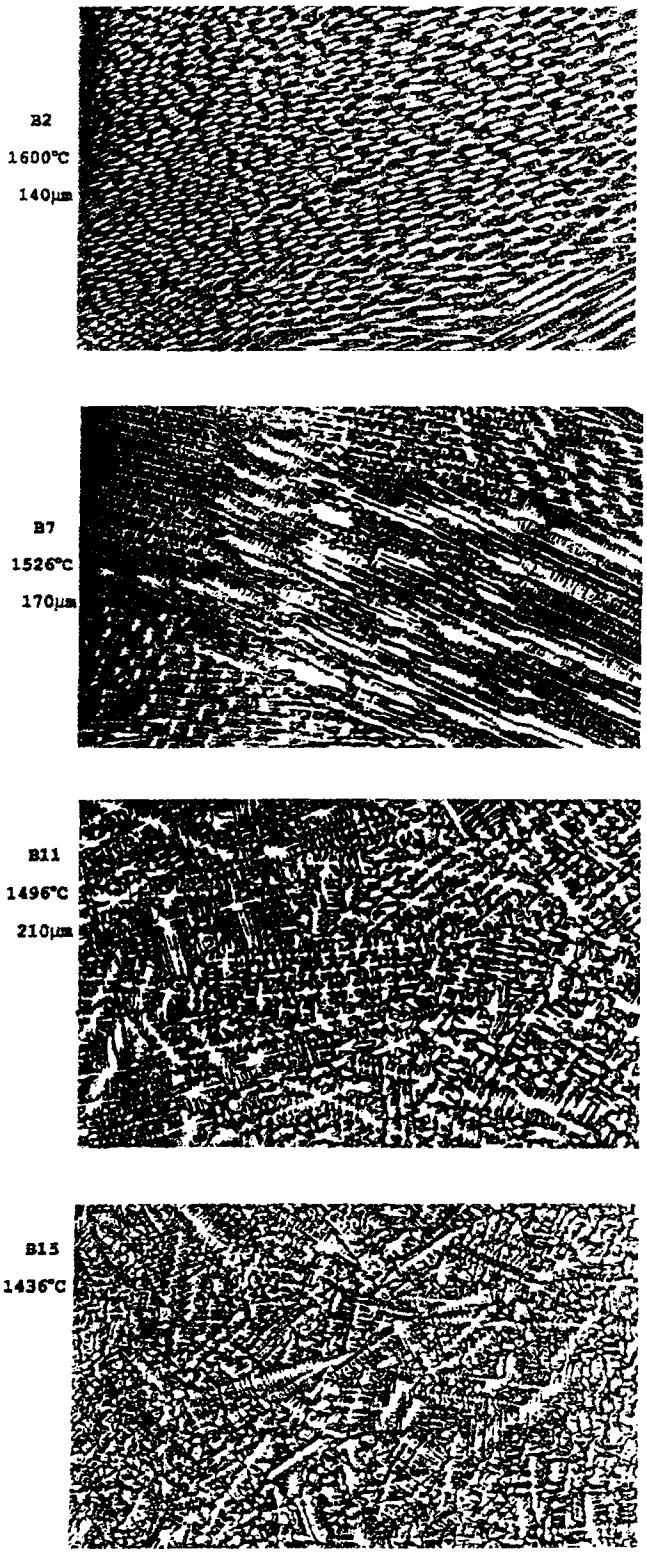

Fig. 10—Microstructure of ingots cast from different temperatures. Primary dendrite arm spacings were measured at 10 mm from the chill zone. Magnification 50 times.

As cooling continued, nucleation occurred when the liquid near the mold wall again cooled down to its nucleation temperature. Because cooling was slow, compared with the drastic chilling effect which produced initial nucleation, few nuclei formed. It appears that the initial chill grains were of δ ferrite, while the subsequent ones were γ grains.[8] Since the nucleation rate was low, a few γ grains nucleated on the mold wall and grew toward the center of the mold while simultaneously thickening. In this temperature range, the growth rate was high relative to the nucleation rate. These conditions favored growth rather than nucleation, resulting in the structure shown in Figure 14(a). Since the number of grains remains constant from the start of nucleation until the grains reach the center, their widths change only slightly as they grow; thus, the grain width ratio usually remains close to unity.

Ingots cast in the temperature range 1476 °C to 1545 °C showed elongated columnar grains, again extending toward the center. The nucleation rate on the surface of the mold was higher than in castings poured in the high-temperature region. The growth rate was lower but still high enough to keep the grains, which nucleated on the surface of the mold, growing until they reached the center of the ingot. These grains outgrew the grains which had unfavorable growth directions, forming a more or less strongly anisotropic macrostructure. That is why, although many grains nucleated on the surface of the mold, only a few of them grew inward to any important extent. It is well known that under these conditions, the grains that survive have a strongly preferred orientation. In face-centered cubic and body-centered cubic structures, for example, all columnar crystals have a ⟨100⟩ axis perpendicular to the mold wall. The crystals with other

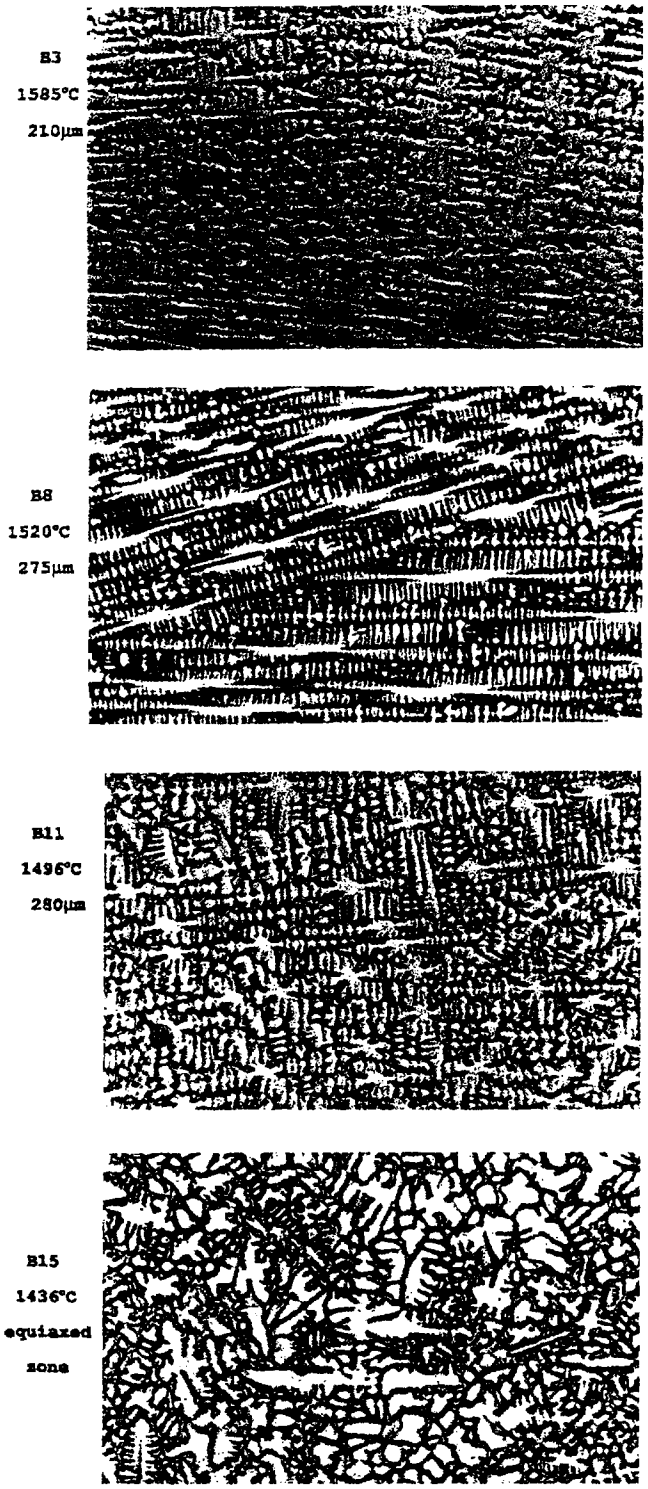

Fig. 11—Microstructure of ingots cast from different temperatures. Primary dendrite arm spacings were measured at 15 mm from the chill zone. Magnification 100 times.

orientations are suppressed, because they do not grow away from the mold as fast as those that are more favorably oriented. This results in the thickening of the advancing grains due to the elimination of unfavorably oriented grains and an increase in the grain width ratio (Figure 14(b)).

With the two ingots cast from temperatures of 1455 °C and 1436 °C, the extent of the equiaxed zone did not allow

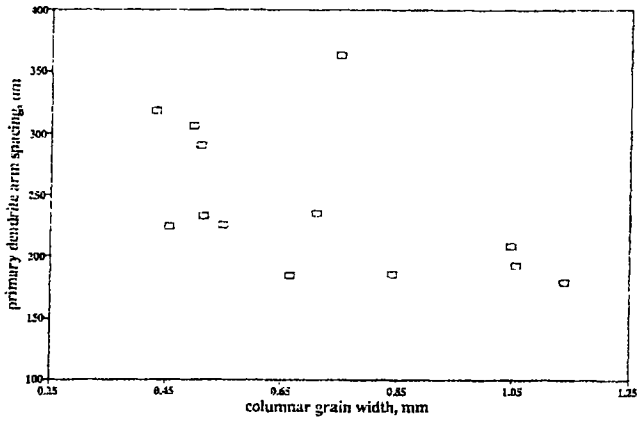

Fig. 12—Change in primary dendrite arm spacing of ingots measured at 15 mm from the chill zone with changes in grain width measured at 6 mm from the chill zone.

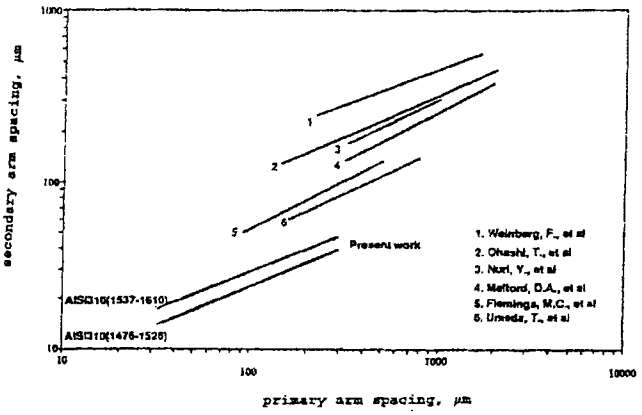

Fig. 13—Comparison between regression lines of secondary and primary arm spacings obtained in this study with similar regression lines found in the literature.[12]

for grain width measurements at 14 mm from the edge of the ingot. This is why there were no grain width ratio data points for these two ingots in Figure 7. However, it can be seen from the macrostructure of the ingot cast from 1436 °C (Figure 2) that the columnar zone of these ingots can be illustrated schematically, as in Figure 14(c).

Since the nucleation rate was high and the growth rate low due to low superheat, the growth of grains stopped shortly after nucleation. Repeated nucleation of new grains occurred ahead of the solid/liquid interface continuously. However, the grains still showed a slight orientation effect due to the relatively high thermal gradients close to the mold wall. This type of columnar zone is actually a transition from the coarse, strongly oriented columnar structure to an isotropic, equiaxed structure and has been referred to as a columnar-equiaxed structure.[3] Due to highly competitive growth conditions, grains do not show much thickening laterally and the resultant grain width ratio is close to unity again, as illustrated in Figure 14(a).

The significance of grain width ratio is that it serves as a useful tool in depicting the shape of the grains and, thus, the nucleation and growth conditions prevailing during the formation of a specific zone in the as-cast structure. However, it is useful only when the structure is columnar or columnar-equiaxed, considering the fact that equiaxed structures are almost always isotropic, *i.e.*, their grain width

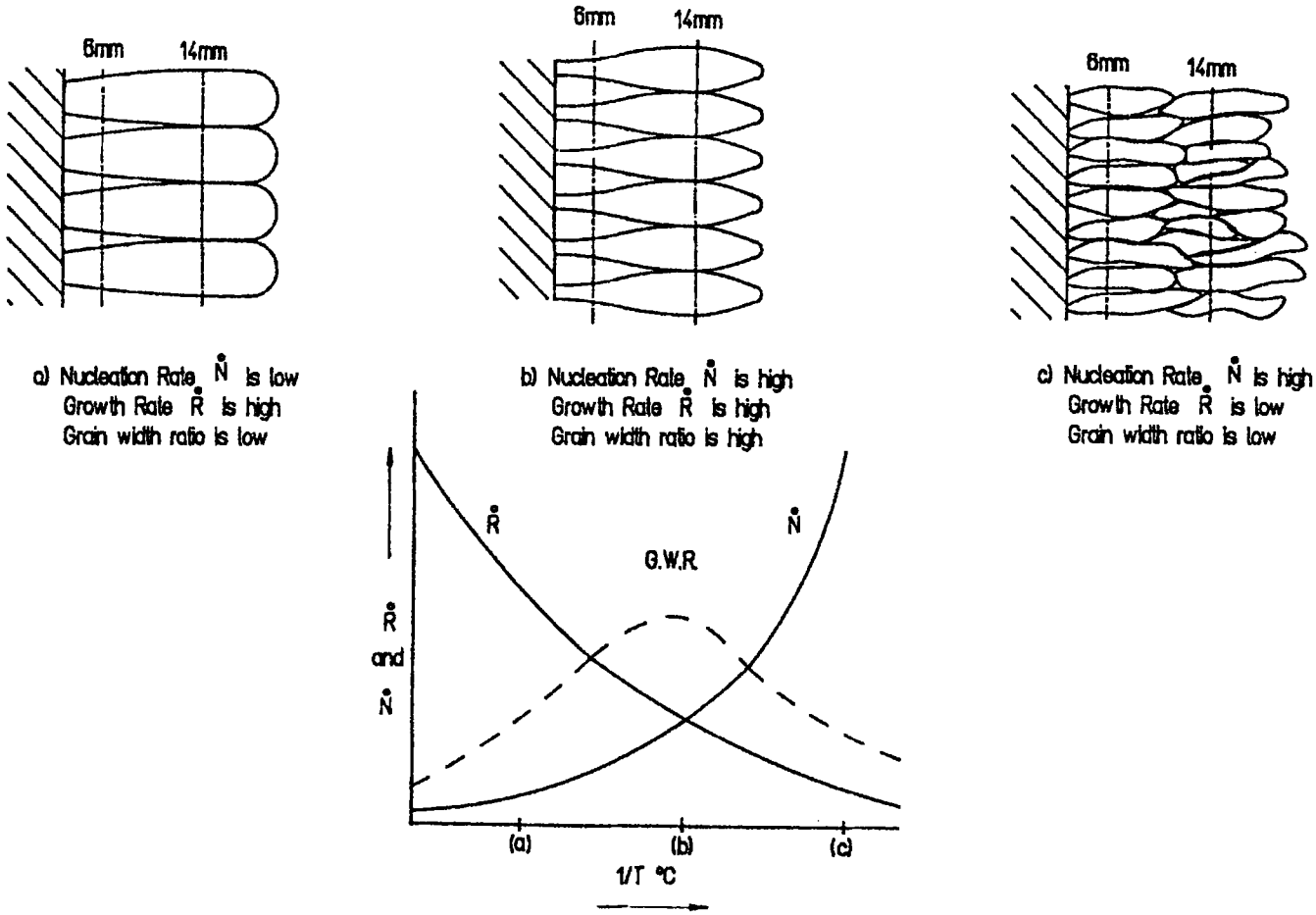

Fig. 14-- Illustrations showing the relationship between grain width ratio and various combinations of nucleation and growth rate conditions and corresponding grain sizes and shapes.

ratio is unity under ideal conditions. But, bearing in mind that in continuous casting processes the as-cast structures are almost always columnar or columnar-equiaxed due to the very high thermal gradients present during solidification, the grain width ratio could be applied to compare the as-cast structures obtained under different conditions. These could include changes in steel composition, slab thickness, casting speed, and so on.

B. *Effect of Superheat on the As-Cast Microstructure*

Figure 12 shows that as the columnar grain width was refined, the primary arm spacings increased, *i.e.*, the microstructure coarsened. This suggests that the nucleation and growth mechanisms for macrograins and primary arms may be different. However, since one comprises the other, they should somehow be related. The micrographs in Figures 10 and 11 show that a coarse grain contained more primary arms than a finer one. As the grains got smaller, the primary arms did not respond to this change by getting smaller. Instead, their number per grain decreased. This can be explained again by considering the role of competition between the nucleation and growth parameters, especially during the early stages of solidification.

As discussed in Section IV.A, at high superheat, the nucleation rate on the mold is very low, due to an insufficient degree of thermal driving force. However, the growth rate is relatively high, because once the nucleus is formed, it is thermally more favorable for it to grow rather than for new nuclei to form because nucleation requires greater amounts of undercooling. Thus, once a grain is nucleated at one point on the surface of the mold, it initially grows laterally to reduce the undercooling in a very narrow region ahead of the mold surface to a very low value. Growth continues until the grain meets the next grain growing in the opposite direction.

As the thermal gradient at the solid/liquid interface decreases, dendritic growth toward the center of the mold starts. This growth in two perpendicular directions most probably takes place concurrently, as illustrated in Figure 15. Since the nucleation rate is higher with lower superheat (low thermal gradient), the number of grains is greater, but the number of primary arms is lower than that obtained with higher superheat over a unit area of mold surface. Low thermal gradients influence the nucleation rate and disturb the strong anisotropy which is present under steep thermal gradients, thus causing a further increase in the average spacing between the arms. Low thermal gradients also lead to the coarsening of dendrite arms that are favorably oriented with respect to the direction of heat flow. This takes place at the expense of arms which are misoriented in this regard.

It, therefore, appears quite possible that thermal gradients are the factor determining the primary arm spacing or the

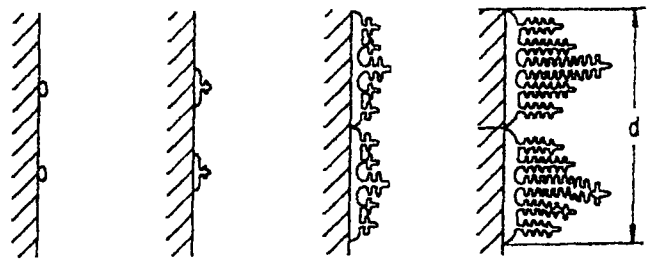

(*a*)

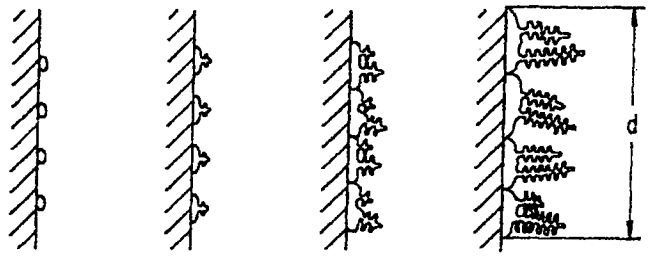

(*b*)

Fig. 15—(*a*) and (*b*) Illustrations showing the influence of superheat on primary arm spacing.

number of arms per unit volume of the solid. This conclusion is consistent with the effect of superheat on grain width ratios.

In his work on the effects of nucleation and constitutional supercooling on the properties of cast steel, Church[10] showed that higher casting temperatures resulted in smaller primary and secondary arm spacings. He found that the difference in cooling rate between two ingots cast with about 100 °C difference in superheat was small, which is in good agreement with the results of this work. However, he also found that the local solidification time for higher casting temperatures was shorter than for lower temperatures, resulting in a shorter mushy zone due to steeper thermal gradients in the mushy region. The relationship between thermal gradient, growth rate, and local solidification time was given[3] by the equation

$$t_f = \frac{\Delta Ts}{GR} \qquad [9]$$

where ΔTs is the solidification range under nonequilibrium cooling conditions and t_f is the local solidification time.

The relationship between dendrite arm spacing and the local solidification time could be expressed as[3]

$$\lambda_1 = at_f^n \qquad [10]$$

This relationship, being exponential, explains the higher rate of increase of primary arm spacing with further decrease in superheat.

V. CONCLUSIONS

From the experimental results obtained in this study, the following main conclusions can be drawn with regard to the changes in macro- and microstructure of AISI 310S stainless steel cast under different conditions.

1. The proportion of the equiaxed zone increased with decreasing alloy superheat. Plots of proportion equiaxed zone against natural logarithm of superheat produced a linear relationship which could be expressed by the equation

$$\text{pct equiaxed zone} = 244.5 + 49.4 \ln \frac{1}{\Delta T}$$

where ΔT is superheat in degrees Celsius.
2. The columnar grain width decreased in an inverse exponential fashion with decreasing superheat. The relationship could be expressed by an equation of the type

$$gw = e^{(a + b/\Delta T)}$$

where a and b are constants and ΔT is superheat.
3. Plots of primary dendrite arm spacing against natural logarithm of the reciprocal of superheat were linear, indicating that the primary dendrite arm spacing increased logarithmically with decreasing superheat.
The mathematical relationship between these two variables was as follows:

$$\lambda_1 = c + d \ln \frac{1}{\Delta T}$$

where c and d are constants and ΔT is superheat.
It is evident from these mathematical relationships that gw and λ_1 responded differently to superheat. While gw increased with superheat, λ_1 decreased.
4. The growth rate of a macrograin at a given superheat was determined by the growth rate of the dendrite making up that specific grain. The growth rate of the dendrite was a function of the distance of the solid-liquid interface from the chill zone. The rate at which columnar grains increased in width at different distances from the chill zone was not constant. This phenomenon was described by the term grain width ratio, which was defined as the ratio of grain widths in flat sections at different distances from the chill zone. This ratio was found to approach unity at high and low superheats as a result of the competition between grain nucleation and growth.
5. The coarsest microstructure was obtained when the rate of heat extraction was very low, which is usually the case as $\Delta T \rightarrow 0$. However, this is also the condition where the proportion of the equiaxed zone approaches 100 pct. Thus, as the proportion of the equiaxed zone increased, due to a decrease in superheat, the primary interarm spacing increased.

REFERENCES

1. G.J. Davies: *Solidification and Casting*, Applied Science Publishers Ltd., Barking, England, 1973.
2. W.A. Tiller, K.A. Jackson, J.W. Rutter, and B. Chalmers: *Acta Metall.*, 1953, vol. 1, pp. 428-37.
3. M.C. Flemings: *Solidification Processing*, McGraw-Hill, New York, NY, 1974.
4. P.R. Beeley: *Foundry Technology*, 4th ed., Butterworth and Co., London, 1982.
5. W.C. Winegard: *Metall. Rev.*, 1961, vol. 6, pp. 57-99.
6. H. Fiegenschuh: Ph.D. Thesis, Technical University of Berlin, Berlin, 1980.

7. D. Apelian and M.R. Ozgu: in *Modelling of Casting and Welding Processes IV*. A.F. Gimaci and G.J. Abbaschian, eds., TMS, Warrendale, PA, 1988.
8. M.S. Ozbayraktar: Ph.D. Thesis, University of the Witwatersrand, Johannesburg, 1992, p. 327.
9. T.E. Roberts, D.P. Kovarik, and R.D. Maier: *AFS Trans.*, 1979, vol. 37, pp. 279-98.
10. N.L. Church: Ph.D. Thesis, Case Institute of Technology, Case Western Reserve University, Cleveland, Ohio, 1965.
11. A. Suzuki and Y. Nakaoka: *J. Jpn. Inst. Met.*, 1969, vol. 33, pp. 658-63.
12. Y. Nuri, F. Weinberg, T. Ohashi, D.A. Melford, M.C. Flemings, and T. Umeda: Trans. I.S.I.J., 1982, vol. 22, pp. 399-407.